Terahertz Reading of Ferroelectric Domain Wall Dielectric Switching

Article *in* ACS Applied Materials & Interfaces · March 2021

DOI: 10.1021/acsami.1c00523

ACS APPLIED MATERIALS & INTERFACES

www.acsami.org

Research Article

Terahertz Reading of Ferroelectric Domain Wall Dielectric Switching

Man Zhang, Zhe Chen, Yajun Yue, Tao Chen, Zhongna Yan, Qinghui Jiang, Bin Yang,* Mirva Eriksson, Jianhua Tang, Dou Zhang,* Zhijian Shen, Isaac Abrahams, and Haixue Yan*

Cite This: https://dx.doi.org/10.1021/acsami.1c00523

Read Online

ACCESS | Metrics & More | Article Recommendations | Supporting Information

ABSTRACT: Ferroelectric domain walls (DWs) are important nanoscale interfaces between two domains. It is widely accepted that ferroelectric domain walls work idly at terahertz (THz) frequencies, consequently discouraging efforts to engineer the domain walls to create new applications that utilize THz radiation. However, the present work clearly demonstrates the activity of domain walls at THz frequencies in a lead-free Aurivillius phase ferroelectric ceramic, $Ca_{0.99}Rb_{0.005}Ce_{0.005}Bi_2Nb_2O_9$, examined using THz-time-domain spectroscopy (THz-TDS). The dynamics of domain walls are different at kHz and THz frequencies. At low frequencies, domain walls work as a group to increase dielectric permittivity. At THz frequencies, the defective nature of domain walls serves to lower the overall dielectric permittivity. This is evidenced by higher dielectric permittivity in the THz band after poling, reflecting decreased domain wall density. An elastic vibrational model has also been used to verify that a single frustrated dipole in a domain wall represents a weaker contribution to the permittivity than its counterpart within a domain. The work represents a fundamental breakthrough in understanding the dielectric contributions of domain walls at THz frequencies. It also demonstrates that THz probing can be used to read domain wall dielectric switching.

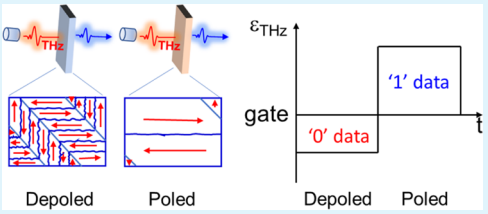

KEYWORDS: *domain wall, ferroelectric, dielectric, lead free, terahertz probe*

1. INTRODUCTION

Ferroelectric materials are commonly used in dielectric capacitors,[1] piezoelectric sensors, actuators,[2,3] and ferroelectric memories for data storage.[4−6] The properties of ferroelectrics are often dominated by the density and activity of their domain walls.[7−11] Domain wall engineering can be used to optimize dielectric,[12−15] piezoelectric,[16,17] and ferroelectric properties[18,19] and hence develop new applications. At present, lead zirconate-titanate (PZT) ceramics are the most widely used commercial ferroelectrics.[20] Experiments have shown that more than 60% of dielectric and piezoelectric responses in PZT ceramics are caused by the contribution of domain walls at room temperature.[21,22] The Landau−Ginzburg−Devonshire theory also reveals that effective piezoelectric response across 90° domain walls is much higher than that in the single-domain region in tetragonal ferroelectrics.[23] Although the contribution from domain walls has been extensively investigated in different ferroelectrics at lower frequencies (kHz), their contribution at terahertz (THz) frequencies has received less attention as it is assumed that the domain walls are only active below 10^{10} Hz.[24] The domain wall dynamics at the THz frequencies are still an open question and a fundamental understanding is a key step toward new applications of ferroelectrics at these higher electromagnetic frequencies.

Aurivillius phase ferroelectrics are good candidate materials for nonvolatile memory and high-temperature piezoelectric sensors due to their fatigue-resistance[5] and high Curie points (T_c),[25] respectively. $CaBi_2Nb_2O_9$ (CBNO) is a ferroelectric with the highest T_c among the Aurivillius phase compounds.[26] Pure CBNO exhibits orthorhombic symmetry in the space group $A2_1am$ with spontaneous polarization (P_s) parallel to the a-axis.[27] Due to its layered structure, ferroelectric switching is restricted to directions perpendicular to the layer axis (c-axis). However, the thermal stability of dielectric permittivity of pure CBNO is low,[28] which limits its commercial use. To improve the thermal stability of dielectric permittivity, a doping approach has been used here in the system $Ca_{0.99}Rb_{0.005}Ce_{0.005}Bi_2Nb_2O_9$ (CBNRC). The dynamics of CBNRC's domain walls at the THz band are investigated by THz-time-domain spectroscopy (THz-TDS) and low-frequency impedance measurements are implemented for complementary analysis. Moreover, an elastic vibrational model has been theoretically constructed to interpret the differential dynamics of a single electric dipole under an alternating electric field in domains and domain walls. The work not only shows that the contribution of ferroelectric domain walls to dielectric permittivity at THz frequencies is non-negligible but also demonstrates the possibility of new

Received: January 9, 2021
Accepted: February 17, 2021

devices based on nondestructive read-out dielectric switching memory, readable by the THz probe.

2. EXPERIMENTAL AND SIMULATION METHOD

$Ca_{0.99}Rb_{0.05}Ce_{0.05}Bi_2Nb_2O_9$ ceramic was prepared by conventional solid-state reaction. Stoichiometric quantities of $CaCO_3$ (99.9% purity), Bi_2O_3 (99.9%), Nb_2O_5 (99.5%), Rb_2CO_3 (99.8%), and CeO_2 (99.9%) were ball milled together for 4 h, using ethanol as the milling medium. The slurry was dried overnight at 80 °C to remove ethanol. The dried mixture was successively calcined at 800 °C for 2 h and 950 °C for 2 h and subsequently remilled for 4 h in ethanol and dried. Poly(vinyl alcohol) (PVA, 5%) was then added to the calcined powder as a binder and the powder was pressed into 13 mm pellets at 150 MPa. The pellets were heated at 650 °C for 2 h to burn out the PVA and then heated up to 1150 °C and held at this temperature for 2 h to sinter the samples. All heating was carried out in air.

The crystal structure of the ceramic was examined by X-ray diffraction (XRD) in flat-plate Bragg−Brentano mode with a PANAlytical X'Pert Pro diffractometer, fitted with an X'Celerator detector using a Ni-filtered Cu Kα radiation (λ = 1.5418 Å). Data were collected in the 2θ range 5−120° in steps of 0.0167°, with an equivalent count time of 200 s per step. Structure refinement was carried out with GSAS suite of programs. The microstructure of the sample was observed using scanning electron microscopy (FEI Inspect-F) equipped with energy-dispersive X-ray spectroscopy (EDX). For electrical property measurements, the samples were polished using SiC paper. Pt (for T_c measurements) or Ag electrodes were painted on both surfaces of the polished samples and fired at 950 °C for 10 min and 300 °C for 30 min, respectively. The temperature dependences of dielectric permittivity and loss were measured at different frequencies using an LCR meter (Agilent, 4284A, Kobe, Hyogo, Japan) connected to a furnace. The current−electric field (I−E) and displacement−electric field (D−E) and strain−electric field (S−E) loops were measured using a ferroelectric hysteresis measurement tester (NPL, U.K.). The piezoelectric coefficient, d_{33}, was measured on a quasi-static d_{33} meter (CAS, ZJ-3B). The samples used for d_{33} measurements were poled in a silicone oil at 180 °C for 20 min under a DC electric field of 13 kV mm^{-1}. Capacitance and loss tangent as a function of frequency were measured using an impedance analyzer (Agilent, 4294A, Hyogo, Japan). The dielectric property of the samples at the THz band was measured using a terahertz time-domain spectroscopy (THz-TDS). The details of the setup and experimental producer are described in the Supporting Information. An elastic vibrational model of an electric dipole under an alternating electric field was constructed and the vibrational dynamics were simulated by Matlab software to demonstrate the differential of a single electric dipole in domain and domain wall.

3. RESULTS AND DISCUSSION

The fitted X-ray diffraction profile of the ground CBNRC ceramic powder is shown in Figure S1, with the crystal and refinement parameters summarized in Table S1. Data are in good agreement with the reference pattern for CBNO (JCPDS #49-0608), with no evidence for secondary phases. The coordinates of CBNO reported by Blake et al.[29] in the space group $A2_1am$ were used as an initial model for structural refinement, yielding refined lattice parameters of a = 5.4758(2) Å, b = 5.4394(2) Å, and c = 24.887(9) Å at room temperature. The resulting unit cell volume is slightly smaller than that of pure CBNO,[29] despite the fact that the Rb^+ cation has a larger ionic radius than Ca^{2+}, while Ce^{3+} has the same ionic radius as Ca^{2+}.[30] This contraction in unit cell volume might be associated with some volatilization of rubidium during the synthesis, but evidence from elemental maps confirms that Rb is present in the sample and is homogeneously distributed (Figure S2). The crystal structure of CBNRC is shown in Figure 1, with the polarization direction indicated. A similar level of ferroelectric distortion,[31,32] defined as $100(a/b - 1)$ is seen in CBNRC (0.66%) compared to CBNO (0.75%).

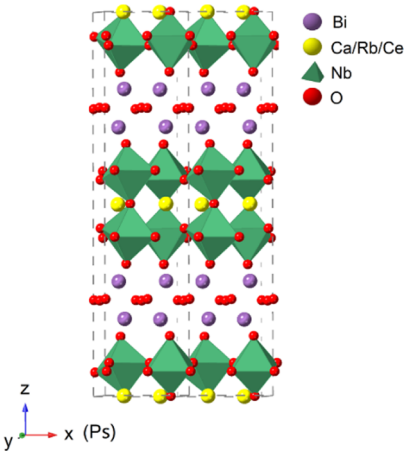

Figure 1. Crystal structure of CBNRC with the polarization direction indicated.

Figure 2a shows the temperature dependence of dielectric permittivity and loss for a CBNRC ceramic. The Curie point

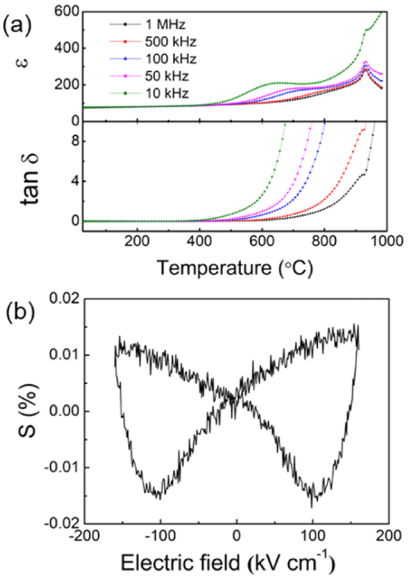

Figure 2. Dielectric and piezoelectric properties of CBNRC ceramics. (a) Temperature dependence of relative dielectric permittivity (ε) and dielectric loss ($\tan\delta$). (b) Strain−electric field (S−E) loop.

(T_c) of CBNRC is 934 °C (±2 °C), slightly lower than the value of 940 °C in pure CBNO, which is consistent with decreased ferroelectric distortion[31] induced by doping. The loss peaks, a few degrees below T_c, can be attributed to the domain wall movement.[26] The frequency dependence of the dielectric permittivity peaks in the temperature range 600−800 °C typically indicates the presence of oxygen vacancies,[26,33] which commonly occur during high-temperature sintering. In Figure 2a, above T_c, the dielectric permittivity at 10 kHz increased with the increasing temperature, but the permittivity decreased at higher frequencies (≥50 kHz). Above T_c, the decrease in dielectric permittivity in the paraelectric phase at high frequency (≥50 kHz) is due to the disappearance of

https://dx.doi.org/10.1021/acsami.1c00523
ACS Appl. Mater. Interfaces XXXX, XXX, XXX−XXX

spontaneous polarization. However, besides the spontaneous polarization and related ferroelectric domains, there are additional dipoles that are active at low frequencies and dominate the contribution to dielectric permittivity at low frequencies. The contributions of these additional dipoles are thermally active and result in the increase of the dielectric permittivity at 10 kHz above T_c. The current−electric field (I−E) and displacement−electric field (D−E) measurements were carried out, yielding an unsaturated D−E hysteresis loop and invisible current peaks related to domain switching in the I−E loop (not shown). These are due to the evidently high coercive field of CBNRC. CBNRC exhibited a piezoelectric coefficient (d_{33}) value of 7.8 pC N^{-1}, after poling under a DC field of 13 kV mm^{-1} in silicone oil for 20 min at 180 °C, confirming ferroelectric domain switching.

As CBNRC has orthorhombic symmetry, spontaneous polarization is developed along the [100] direction. Both 90 and 180° domain walls, which can be referred to as non-180° and 180° domain walls, are permissible in grains of the ceramic. The motion of 180° domain walls will affect only the dielectric properties while the motion of non-180° domain walls will affect both dielectric and piezoelectric properties.[21,34] Further confirmation of non-180° domain wall switching is seen in the butterfly shape of the strain−electric field (S−E) loop (Figure 2b). The switching of non-180° domains upon application of the electric field is the major mechanism contributing to the butterfly-shaped S−E loop.[35]

To understand the contribution of domain walls to dielectric properties, dielectric permittivity and loss were characterized using impedance spectroscopy and THz-TDS, the results of which are shown in Figure 3. Figure 3a shows the dielectric

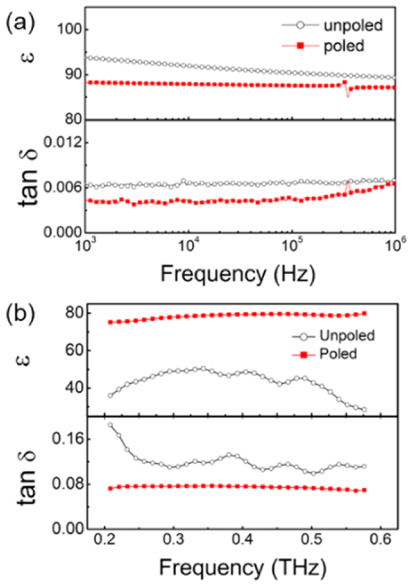

Figure 3. Dielectric properties of CBNRC ceramic at different frequencies. (a) Dielectric properties at kHz frequencies. (b) Dielectric properties at THz frequencies.

permittivity and loss of a CBNRC ceramic in unpoled and poled states in the frequency range of 1 kHz to 1 MHz. The poling process induced irreversible domain wall switching and caused a decrease in domain wall density in the poled sample. Compared with the unpoled sample, the dielectric permittivity of the poled sample decreased, which indicates that the switching of the non-180° domain walls decreases the domain wall density and hence lowers the dielectric response at low frequency after poling.[36] The peaks in ε_r and tan δ plots of the poled ceramic are attributed to the piezoelectric effect. Figure 3b shows the relative dielectric permittivity and dielectric loss of poled and unpoled CBNRC ceramic at THz frequencies. Relative permittivity is lower at these high frequencies than that at lower frequencies, which is consistent with the fact that there are different dipoles in dielectrics and the dipoles with long relaxation time cannot follow the AC field at higher frequencies.[37−39] Moreover, the dielectric loss at THz frequencies is higher than that at low frequencies, which can be attributed to the dielectric relaxation mechanism happening close to the measured THz band. There are many different polarizations in CBNRC, and some polarizations are active and their relaxation frequencies are close to the measured THz frequencies, which causes dielectric relaxation and related high loss at the THz frequencies. As these relaxation scenarios happen only at the higher frequencies, low-frequency measurements are not able to reflect these high-frequency relaxation mechanisms. As shown in Figure 3b, the poled CBNRC sample surprisingly exhibits higher dielectric permittivity and lower dielectric loss than the unpoled sample in the THz frequency range. This appears to contradict the traditional view that the domain wall contribution dies above 10^{10} Hz.[24,37,40] It is worth noting that the unpoled sample shows Fabry−Perot (FP) oscillations,[41] but the poled sample does not. The high permittivity of the poled sample causes a significant time delay in the wave propagation inside the sample. This time delay is longer than the detector repetition rate of the THz system and therefore FP effects are undetectable. For the unpoled sample, equal intervals of ∼48 GHz in the lower THz band are observed and matched to the sample thickness (440 μm) and permittivity (∼50). The decreased permittivity at higher THz frequencies (>0.48 THz) causes a shorter time delay in wave propagation inside the sample, resulting in an increase in the interval frequency of FP oscillations. The FP oscillations show relatively shifted frequencies in permittivity and loss tangent, caused by the higher loss tangent values of the unpoled sample.[41]

To explain the differences in dielectric behavior of CBNRC ceramic in different states (poled and unpoled) and in different frequency ranges, the domain wall contribution was analyzed from the macroscopic and microscopic perspectives. As described above, the dielectric permittivity mainly consists of contributions from lattice-level intrinsic polarization, defects, and domain wall motion. Thus, the dielectric permittivity can be denoted as

$$\varepsilon = \varepsilon_{in} + \varepsilon_{def} + \varepsilon_{DW-non180} + \varepsilon_{DW-180}$$

where ε_{in} is the intrinsic contribution to permittivity, ε_{def} is a point defect contribution (mainly from oxygen vacancies, V_O''), $\varepsilon_{DW\text{-}non180}$ is the non-180° domain wall contribution, and $\varepsilon_{DW\text{-}180}$ is the 180° domain wall contribution. While the relaxation frequency of intrinsic polarization lies beyond the THz frequencies,[39,42] the point defects in CBNRC are mainly active at low frequencies, which is supported by the fact that the V_O'' related dielectric peaks are greatly weakened with increasing frequency in Figure 2a. The domain walls, however, will contribute to dielectric permittivity differently at different frequencies. Figure 4a,b shows illustrations of non-180° and 180° ferroelectric domains with details of the corresponding domain walls shown in Figure 4c,d. To minimize the free energy with the gradient change of polarization across the

https://dx.doi.org/10.1021/acsami.1c00523
ACS Appl. Mater. Interfaces XXXX, XXX, XXX−XXX

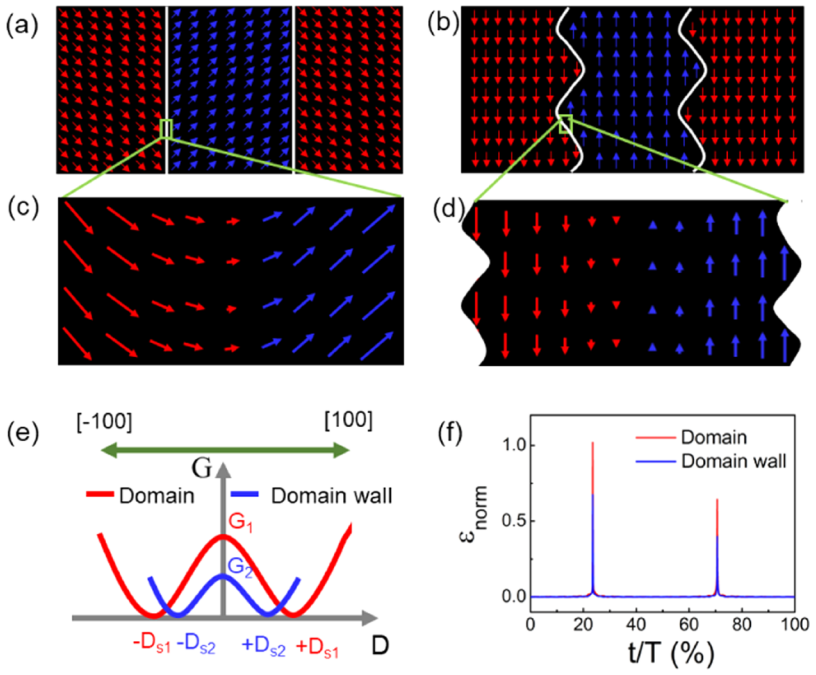

Figure 4. Illustration of ferroelectric domains and domain walls and their dynamics. (a) Non-180° domains; (b) 180° domains; (c) non-180° domain walls; (d) 180° domain walls; (e) variation of free energy of domain and domain walls with displacement; and (f) simulated permittivity contribution of a single dipole in a domain (red) or domain wall (blue), where ε_{norm} is the normalized permittivity $\varepsilon/\varepsilon_{max(domain)}$ and the x-axis is the percentage of the cycle period.

domain wall, weak dipoles (frustrated dipoles) develop within the domain walls (Figure 4c,4d).[18,43−45] Figure 4e shows a schematic representation of the variation of Gibbs free energy, G, with electric displacement for domains and domain walls, the polar vectors of which are in the [−100] and [100] directions. At temperatures lower than T_c, there are two minima for domains and domain walls on the free-energy profile[46] and thus the ferroelectric phase is stable. From the thermodynamic theory, the dielectric displacement is the first derivative of G with respect to the electric field $\left(D = \frac{\partial G}{\partial E}\right)$. As the domain walls are made up of frustrated dipoles within nanoscaled interfaces, the dielectric displacement of domain walls D_{S2} is smaller than that of domains D_{S1}.[16] At low frequencies, all of the dipoles within the domain walls are able to follow the AC field and each domain wall is active as a group. The non-180° domain walls will increase dielectric permittivity[47] and the 180° domain walls will decrease permittivity because of their clamping effect.[48−50] The decreased dielectric permittivity in poled samples at low frequencies (Figure 4a) indicates that the positive contribution from $\varepsilon_{DW\text{-}non180}$ is the dominant factor between the competitive effects of $\varepsilon_{DW\text{-}non180}$ and $\varepsilon_{DW\text{-}180}$. At THz frequencies, the local lattices within domain walls are active as single frustrated dipoles instead of a group. The permittivity of a single frustrated dipole in the domain wall is smaller than its counterpart in the domain. The contribution of a single dipole in the lattice (either in a domain or a domain wall) to dielectric permittivity can be calculated using an elastic vibration model (see Figure 4f and the Supporting Information).[42] The contribution to permittivity from a dipole in a domain is higher than that from one in a domain wall. This is in good agreement with our experimental results that the dielectric permittivity is higher in the poled ceramic at THz frequencies due to its lower domain wall density.

As the domain wall dynamics of ferroelectrics are active in the THz band, they can be utilized in new and viable applications, such as low-loss dielectrics and nondestructive read-out ferroelectric memory driven by THz technologies through domain wall engineering. For new dielectrics to be used at THz frequencies, materials should have moderate dielectric permittivity and low dielectric loss.[51] Figure S6 displays the dielectric properties of different ferroelectric materials summarized at 0.5 THz from the literature. The CBNRC ceramic produced in this work has medium dielectric permittivity and low dielectric loss in the THz band. The dielectric permittivity of CBNRC doubles on poling and the dielectric loss decreases, indicating its suitability for dielectric applications at these frequencies. A proposed application for this effect is a nondestructive read-out dielectric memory. Previously, the read-out of ferroelectric memory has been mainly based on destructive bipolar[52] or domain-wall-type resistance[53] switching. The disadvantage of the former technique is its destructive nature, while the latter is limited by the low current generated from these switches, which is insufficient to drive read-out circuits. Figure 5 shows the proposed mechanism of THz reading of dielectric switching memory, where dielectric permittivity can be modulated by domain wall dielectric switching through poling and depoling. The morphology of 90 and 180° domain walls is demonstrated using straight lines and curves.[54] Here, poling or depoling is used to facilitate the writing process; the poled state is achieved by an applied DC field and the depoled state is achieved by a reverse bias DC field because a poled ferroelectric can be depolarized when the reversal field is applied at the negative coercive field, which enables to achieve a reversed and erasable memory. The domain wall density is low in the poled state and high in the depoled state, reflective of high and low dielectric permittivity at THz frequencies, respectively. For dielectric memory applications, the modu-

https://dx.doi.org/10.1021/acsami.1c00523
ACS Appl. Mater. Interfaces XXXX, XXX, XXX−XXX

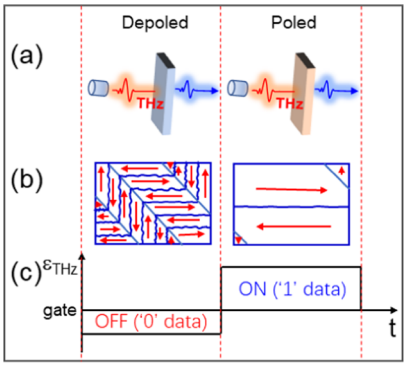

Figure 5. Illustration of nondestructive read-out dielectric switching memory. (a) Schematic setup of THz reading technology; (b) domain wall density change in depoled and poled ferroelectric; and (c) THz reading of off/on (0/1) positions. Dashed lines denote depoled and poled states.

lated permittivity is compared with a set "gate" permittivity and then marked as the "off" state if it is below or "on" if it is above this value. These off and on states correspond to "0" and "1" digital positions, which can be spontaneously read by THz probe signaling. This nondestructive read mechanism could pave the way for the development of next-generation THz ferroelectric devices.

4. CONCLUSIONS

In summary, the dynamics of domain walls in the CBNRC ferroelectric ceramic have been read using THz-time-domain spectroscopy, which are compared with the contribution from the low-frequency impedance spectroscopy. The results show that non-180° domain walls actively contribute to high permittivity at the low frequencies. At the THz band, domain walls are nonactive as a group due to their long relaxation time, and they work as defective interfaces originating from their frustrated dipoles. These unfulfilled dipoles in the domain walls contribute less to the permittivity compared with their counterparts in domains. The experimental results are theoretically supported by an elastic vibration model. The work here shows that field-induced changes in domain wall density are detectable at high frequencies and are related to lattice-level dynamics of dipoles in ferroelectrics. This observation could lead to new THz frequency applications for ferroelectrics such as domain wall dielectric switching memory.

■ ASSOCIATED CONTENT

Supporting Information

The Supporting Information is available free of charge at https://pubs.acs.org/doi/10.1021/acsami.1c00523.

Experimental procedures, XRD results and refined data, simulation of permittivity for a single dipole in domain and domain wall, and comparison of dielectric properties between the current material in this paper with other ferroelectrics (PDF)

■ AUTHOR INFORMATION

Corresponding Authors

Bin Yang − *Faculty of Science and Engineering, University of Chester, Chester CH2 4NU, United Kingdom*; Email: b.yang@chester.ac.uk

Dou Zhang − *State Key Laboratory of Powder Metallurgy, Central South University, Changsha 410083, China*; orcid.org/0000-0001-8555-2784; Email: dzhang@csu.edu.cn

Haixue Yan − *School of Engineering and Materials Science, Queen Mary University of London, London E1 4NS, United Kingdom*; orcid.org/0000-0002-4563-1100; Email: h.x.yan@qmul.ac.uk

Authors

Man Zhang − *School of Engineering and Materials Science, Queen Mary University of London, London E1 4NS, United Kingdom*

Zhe Chen − *Faculty of Science and Engineering, University of Chester, Chester CH2 4NU, United Kingdom; College of Electronic Information Engineering, South-Central University for Nationalities, Wuhan 430074, China*

Yajun Yue − *School of Biological and Chemical Sciences, Queen Mary University of London, London E1 4NS, United Kingdom*

Tao Chen − *School of Biological and Chemical Sciences, Queen Mary University of London, London E1 4NS, United Kingdom*

Zhongna Yan − *School of Biological and Chemical Sciences, Queen Mary University of London, London E1 4NS, United Kingdom; State Key Laboratory of Powder Metallurgy, Central South University, Changsha 410083, China*

Qinghui Jiang − *School of Materials Science and Engineering, Huazhong University of Science and Technology, Wuhan 430074, China*

Mirva Eriksson − *Department of Materials and Environmental Chemistry, Stockholm University, SE-106 91 Stockholm, Sweden*

Jianhua Tang − *Cancer Research UK Manchester Institute, The University of Manchester, Manchester SK10 4TG, United Kingdom*

Zhijian Shen − *Department of Materials and Environmental Chemistry, Stockholm University, SE-106 91 Stockholm, Sweden*

Isaac Abrahams − *School of Biological and Chemical Sciences, Queen Mary University of London, London E1 4NS, United Kingdom*; orcid.org/0000-0002-8606-6056

Complete contact information is available at: https://pubs.acs.org/10.1021/acsami.1c00523

Author Contributions

The manuscript was written through contributions of all authors. All authors have given approval to the final version of the manuscript.

Funding

H.Y. thanks the financial support from the Engineering and Physical Sciences Research Council (EPSRC) (MASSIVE Project, EP/L017695/1) and the Royal Society for a Newton Advanced Fellowship award (NAF\R1\201126). M.Z. thanks the financial support from China Scholarship Council (CSC, 201706370172). D.Z. thanks the National Natural Science Foundation of China (Grant No. U19A2087) for the financial support. D.Z. and H.Y. thank the financial support from Guangzhou Guangding Technology Group Co. Ltd.

Notes

The authors declare no competing financial interest.

https://dx.doi.org/10.1021/acsami.1c00523
ACS Appl. Mater. Interfaces XXXX, XXX, XXX−XXX

REFERENCES

(1) Prateek; Thakur, V. K.; Gupta, R. K. Recent Progress on Ferroelectric Polymer-Based Nanocomposites for High Energy Density Capacitors: Synthesis, Dielectric Properties, and Future Aspects. *Chem. Rev.* **2016**, *116*, 4260−4317.

(2) Muralt, P. Ferroelectric Thin Films for Micro-Sensors and Actuators: A Review. *J. Micromech. Microeng.* **2000**, *10*, No. 136.

(3) Zhang, S.; Yu, F. Piezoelectric Materials for High Temperature Sensors. *J. Am. Ceram. Soc.* **2011**, *94*, 3153−3170.

(4) De Araujo, C. A. P.; Cuchiaro, J. D.; Mc Millan, D. L.; Scott, M. C.; Scott, J. F. Fatigue-Free Ferroelectric Capacitors with Platinum Electrodes. *Nature* **1995**, *374*, 627−629.

(5) Park, B. H.; Kang, B. S.; Bu, S. D.; Noh, T. W.; Lee, J.; Jo, W. Lanthanum-Substituted Bismuth Titanate for Use in Non-Volatile Memories. *Nature* **1999**, *401*, 682−684.

(6) Ma, C.; Luo, Z.; Huang, W.; Zhao, L.; Chen, Q.; Lin, Y.; Liu, X.; Chen, Z.; Liu, C.; Sun, H.; Jin, X.; Yin, Y.; Li, X. Sub-Nanosecond Memristor Based on Ferroelectric Tunnel Junction. *Nat. Commun.* **2020**, *11*, No. 1439.

(7) Li, J. Y.; Rogan, R. C.; Üstündag, E.; Bhattacharya, K. Domain Switching in Polycrystalline Ferroelectric Ceramics. *Nat. Mater.* **2005**, *4*, 776−781.

(8) Jesse, S.; Rodriguez, B. J.; Choudhury, S.; Baddorf, A. P.; Vrejoiu, I.; Hesse, D.; Alexe, M.; Eliseev, E. A.; Morozovska, A. N.; Zhang, J.; Chen, L. Q.; Kalinin, S. V. Direct Imaging of the Spatial and Energy Distribution of Nucleation Centres in Ferroelectric Materials. *Nat. Mater.* **2008**, *7*, 209−215.

(9) Ma, H.; Gao, W.; Wang, J.; Wu, T.; Yuan, G.; Liu, J.; Liu, Z. Ferroelectric Polarization Switching Dynamics and Domain Growth of Triglycine Sulfate and Imidazolium Perchlorate. *Adv. Electron. Mater.* **2016**, *2*, No. 1600038.

(10) Li, Y.; Sun, N.; Li, X.; Du, J.; Chen, L.; Gao, H.; Hao, X.; Cao, M. Multiple Electrical Response and Enhanced Energy Storage Induced by Unusual Coexistent-Phase Structure in Relaxor Ferroelectric Ceramics. *Acta Mater.* **2018**, *146*, 202−210.

(11) Li, Y.; Sun, N.; Du, J.; Li, X.; Hao, X. Stable Energy Density of a PMN-PST Ceramic from Room Temperature to Its Curie Point Based on the Synergistic Effect of Diversified Energy. *J. Mater. Chem. C* **2019**, *7*, 7692−7699.

(12) Pan, H.; Li, F.; Liu, Y.; Zhang, Q.; Wang, M.; Lan, S.; Zheng, Y.; Ma, J.; Gu, L.; Shen, Y.; Yu, P.; Zhang, S.; Chen, L. Q.; Lin, Y. H.; Nan, C. W. Ultrahigh−Energy Density Lead-Free Dielectric Films via Polymorphic Nanodomain Design. *Science* **2019**, *365*, 578−582.

(13) Qi, H.; Zuo, R.; Xie, A.; Tian, A.; Fu, J.; Zhang, Y.; Zhang, S. Ultrahigh Energy-Storage Density in $NaNbO_3$-Based Lead-Free Relaxor Antiferroelectric Ceramics with Nanoscale Domains. *Adv. Funct. Mater.* **2019**, *29*, No. 1903877.

(14) Luo, N.; Han, K.; Cabral, M. J.; Liao, X.; Zhang, S.; Liao, C.; Zhang, G.; Chen, X.; Feng, Q.; Li, J. F.; Wei, Y. Constructing Phase Boundary in $AgNbO_3$ Antiferroelectrics: Pathway Simultaneously Achieving High Energy Density and Efficiency. *Nat. Commun.* **2020**, *11*, No. 4824.

(15) Gu, Z.; Pandya, S.; Samanta, A.; Liu, S.; Xiao, G.; Meyers, C. J. G.; Damodaran, A. R.; Barak, H.; Dasgupta, A.; Saremi, S.; Polemi, A.; Wu, L.; Podpirka, A. A.; Will-Cole, A.; Hawley, C. J.; Davies, P. K.; York, R. A.; Grinberg, I.; Martin, L. W.; Spanier, J. E. Resonant Domain-Wall-Enhanced Tunable Microwave Ferroelectrics. *Nature* **2018**, *560*, 622−627.

(16) Li, F.; Lin, D.; Chen, Z.; Cheng, Z.; Wang, J.; Li, C.; Xu, Z.; Huang, Q.; Liao, X.; Chen, L. Q.; Shrout, T. R.; Zhang, S. Ultrahigh Piezoelectricity in Ferroelectric Ceramics by Design. *Nat. Mater.* **2018**, *17*, 349−354.

(17) Li, P.; Zhai, J.; Shen, B.; Zhang, S.; Li, X.; Zhu, F.; Zhang, X. Ultrahigh Piezoelectric Properties in Textured $(K,Na)NbO_3$-Based Lead-Free Ceramics. *Adv. Mater.* **2018**, *30*, No. 1705171.

(18) Liu, S.; Cohen, R. E. Origin of Stationary Domain Wall Enhanced Ferroelectric Susceptibility. *Phys. Rev. B* **2017**, *95*, No. 094102.

(19) Spaldin, N. A. Fundamental Size Limits in Ferroelectricity. *Science* **2004**, *304*, 1606−1607.

(20) Kingon, A. I.; Srinivasan, S. Lead Zirconate Titanate Thin Films Directly on Copper Electrodes for Ferroelectric, Dielectric and Piezoelectric Applications. *Nat. Mater.* **2005**, *4*, 233−237.

(21) Zhang, Q. M.; Wang, H.; Kim, N.; Cross, L. E. Direct Evaluation of Domain-Wall and Intrinsic Contributions to the Dielectric and Piezoelectric Response and Their Temperature Dependence on Lead Zirconate-Titanate Ceramics. *J. Appl. Phys.* **1994**, *75*, 454−459.

(22) Xu, F.; Trolier-McKinstry, S.; Ren, W.; Xu, B.; Xie, Z. L.; Hemker, K. J. Domain Wall Motion and Its Contribution to the Dielectric and Piezoelectric Properties of Lead Zirconate Titanate Films. *J. Appl. Phys.* **2001**, *89*, 1336−1348.

(23) Morozovska, A. N.; Eliseev, E. A.; Varenyk, O. V.; Kalinin, S. V. Effective Piezoelectric Response of Twin Walls in Ferroelectrics. *J. Appl. Phys.* **2013**, *113*, No. 187222.

(24) Tsurumi, T.; Li, J.; Hoshina, T.; Kakemoto, H.; Nakada, M.; Akedo, J. Ultrawide Range Dielectric Spectroscopy of $BaTiO_3$-Based Perovskite Dielectrics. *Appl. Phys. Lett.* **2007**, *91*, No. 182905.

(25) Yan, H.; Zhang, H.; Ubic, R.; Reece, M. J.; Liu, J.; Shen, Z.; Zhang, Z. A Lead-Free High-Curie-Point Ferroelectric Ceramic, $CaBi_2Nb_2O_9$. *Adv. Mater.* **2005**, *17*, 1261−1265.

(26) Yan, H.; Zhang, H.; Reece, M. J.; Dong, X. Thermal Depoling of High Curie Point Aurivillius Phase Ferroelectric Ceramics. *Appl. Phys. Lett.* **2005**, *87*, No. 082911.

(27) Newnham, R. E.; Wolfe, R. W.; Dorrian, J. F. Structural Basis of Ferroelectricity in the Bismuth Titanate Family. *Mater. Res. Bull.* **1971**, *6*, 1029−1039.

(28) Zhang, H.; Yan, H.; Reece, M. J. Microstructure and Electrical Properties of Aurivillius Phase $(CaBi_2Nb_2O_9)_{1-x}(BaBi_2Nb_2O_9)_x$ Solid Solution. *J. Appl. Phys.* **2010**, *108*, No. 014109.

(29) Blake, S. M.; Falconer, M. J.; McCreedy, M.; Lightfoot, P. Cation Disorder in Ferroelectric Aurivillius Phases of the Type $Bi_2ANb_2O_9$ (A = Ba, Sr, Ca). *J. Mater. Chem.* **1997**, *7*, 1609−1613.

(30) Shannon, R. D. Revised Effective Ionic Radii and Systematic Studies of Interatomic Distances in Halides and Chalcogenides. *Acta Crystallogr., Sect. A* **1976**, *32*, 751−767.

(31) Viola, G.; Boon Chong, K.; Eriksson, M.; Shen, Z.; Zeng, J.; Yin, Q.; Kan, Y.; Wang, P.; Ning, H.; Zhang, H.; Fitzpatrick, M. E.; Reece, M. J.; Yan, H. Effect of Grain Size on Domain Structures, Dielectric and Thermal Depoling of Nd-Substituted Bismuth Titanate Ceramics. *Appl. Phys. Lett.* **2013**, *103*, No. 182903.

(32) Zhao, Z.; Buscaglia, V.; Viviani, M.; Buscaglia, M. T.; Mitoseriu, L.; Testino, A.; Nygren, M.; Johnsson, M.; Nanni, P. Grain-Size Effects on the Ferroelectric Behavior of Dense Nanocrystalline $BaTiO_3$ Ceramics. *Phys. Rev. B* **2004**, *70*, No. 024107.

(33) Tan, Y.; Zhang, J.; Wu, Y.; Wang, C.; Koval, V.; Shi, B.; Ye, H.; McKinnon, R.; Viola, G.; Yan, H. Unfolding Grain Size Effects in Barium Titanate Ferroelectric Ceramics. *Sci. Rep.* **2015**, *5*, No. 9953.

(34) Zheng, T.; Wu, J.; Cheng, X.; Wang, X.; Zhang, B.; Xiao, D.; Zhu, J.; Wang, X.; Lou, X. High Strain in $(K_{0.40}Na_{0.60})(Nb_{0.955}Sb_{0.045})$-$O_3$-$Bi_{0.50}Na_{0.50}ZrO_3$ Lead-Free Ceramics with Large Piezoelectricity. *J. Mater. Chem. C* **2014**, *2*, 8796−8803.

(35) Viola, G.; Saunders, T.; Wei, X.; Chong, K. B.; Luo, H.; Reece, M. J.; Yan, H. Contribution of Piezoelectric Effect, Electrostriction and Ferroelectric/Ferroelastic Switching to Strain-Electric Field Response of Dielectrics. *J. Adv. Dielectr.* **2013**, *03*, No. 1350007.

(36) Tan, Y.; Viola, G.; Koval, V.; Yu, C.; Mahajan, A.; Zhang, J.; Zhang, H.; Zhou, X.; Tarakina, N. V.; Yan, H. On the Origin of Grain Size Effects in $Ba(Ti_{0.96}Sn_{0.04})O_3$ Perovskite Ceramics. *J. Eur. Ceram. Soc.* **2019**, *39*, 2064−2075.

(37) Hoshina, T.; Kigoshi, Y.; Hatta, S.; Teranishi, T.; Takeda, H.; Tsurumi, T. Size Effect and Domain-Wall Contribution of Barium Titanate Ceramics. *Ferroelectrics* **2010**, *402*, 29−36.

(38) Zhu, L.; Wang, Q. Novel Ferroelectric Polymers for High Energy Density and Low Loss Dielectrics. *Macromolecules* **2012**, *45*, 2937−2954.

https://dx.doi.org/10.1021/acsami.1c00523
ACS Appl. Mater. Interfaces XXXX, XXX, XXX−XXX

(39) Wu, J.; Sun, W.; Meng, N.; Zhang, H.; Koval, V.; Zhang, Y.; Donnan, R.; Yang, B.; Zhang, D.; Yan, H. Terahertz Probing Irreversible Phase Transitions Related to Polar Clusters in $Bi_{0.5}Na_{0.5}TiO_3$-Based Ferroelectric. *Adv. Electron. Mater.* **2020**, *6*, No. 1901373.
(40) Tsykalov, V. G.; Poplavko, Y. M. Permittivity Dispersion of Various Ferro-and Antiferroelectrics in the Millimetre Wave-Length Range above the Curie Point. *Izv. Akad. Nauk SSSR* **1970**, *34*, 2586−2589.
(41) Yang, B.; Wylde, R. J.; Martin, D. H.; Goy, P.; Donnan, R. S.; Caroopen, S. Determination of the Gyrotropic Characteristics of Hexaferrite Ceramics from 75 to 600 GHz. *IEEE Trans. Microwave Theory Tech.* **2010**, *58*, 3587−3597.
(42) Barsoum, M. *Fundamentals of Ceramics*; CRC Press, 2019.
(43) Lee, D.; Behera, R. K.; Wu, P.; Xu, H.; Sinnott, S. B.; Phillpot, S. R.; Chen, L. Q.; Gopalan, V.; et al. Mixed Bloch-Néel-Ising Character of 180° ferroelectric Domain Walls. *Phys. Rev. B* **2009**, *80*, No. 149904.
(44) Jia, C. L.; Mi, S. B.; Urban, K.; Vrejoiu, I.; Alexe, M.; Hesse, D. Atomic-Scale Study of Electric Dipoles near Charged and Uncharged Domain Walls in Ferroelectric Films. *Nat. Mater.* **2008**, *7*, 57−61.
(45) Nelson, C. T.; Winchester, B.; Zhang, Y.; Kim, S. J.; Melville, A.; Adamo, C.; Folkman, C. M.; Baek, S. H.; Eom, C. B.; Schlom, D. G.; Chen, L. Q.; Pan, X. Spontaneous Vortex Nanodomain Arrays at Ferroelectric Heterointerfaces. *Nano Lett.* **2011**, *11*, 828−834.
(46) Lines, M. E.; Glass, A. M. *Principles and Applications of Ferroelectrics and Related Materials*; Oxford University Press, 2001.
(47) Xu, R.; Karthik, J.; Damodaran, A. R.; Martin, L. W. Stationary Domain Wall Contribution to Enhanced Ferroelectric Susceptibility. *Nat. Commun.* **2014**, *5*, No. 3120.
(48) Drougard, M. E.; Young, D. R. Domain Clamping Effect in Barium Titanate Single Crystals. *Phys. Rev.* **1954**, *94*, No. 1561.
(49) Zhang, H.; Yang, B.; Yan, H.; Abrahams, I. Isolation of a Ferroelectric Intermediate Phase in Antiferroelectric Dense Sodium Niobate Ceramics. *Acta Mater.* **2019**, *179*, 255−261.
(50) Yan, Z.; Zhang, D.; Zhou, X.; Zhang, M.; Yue, Y.; Zhang, L.; Xue, G.; Luo, H.; Abrahams, I.; Yan, H. Phase Transitions in $RbPrNb_2O_7$, a Layer Structured Ferroelectric with a High Curie Point. *Acta Mater.* **2020**, *200*, 971−979.
(51) Kong, L. B.; Li, S.; Zhang, T. S.; Zhai, J. W.; Boey, F. Y. C.; Ma, J. Electrically Tunable Dielectric Materials and Strategies to Improve Their Performances. *Prog. Mater. Sci.* **2010**, *55*, 840−893.
(52) Blom, P. W. M.; Wolf, R. M.; Cillessen, J. F. M.; Krijn, M. P. C. M. Ferroelectric Schottky Diode. *Phys. Rev. Lett.* **1994**, *73*, No. 2107.
(53) Jiang, J.; Bai, Z. L.; Chen, Z. H.; He, L.; Zhang, D. W.; Zhang, Q. H.; Shi, J. A.; Park, M. H.; Scott, J. F.; Hwang, C. S.; Jiang, A. Q. Temporary Formation of Highly Conducting Domain Walls for Non-Destructive Read-out of Ferroelectric Domain-Wall Resistance Switching Memories. *Nat. Mater.* **2018**, *17*, 49−55.
(54) Cheng, S. Y.; Ho, N. J.; Lu, H. Y. Transformation-Induced Twinning: The 90° and 180° Ferroelectric Domains in Tetragonal Barium Titanate. *J. Am. Ceram. Soc.* **2006**, *89*, 2177−2187.

https://dx.doi.org/10.1021/acsami.1c00523
ACS Appl. Mater. Interfaces XXXX, XXX, XXX−XXX